PNAS RESEARCH ARTICLE | NEUROSCIENCE APPLIED MATHEMATICS OPEN ACCESS

Overcoming the space clamp effect: Reliable recovery of local and effective synaptic conductances of neurons

Ziling Wang[a,b,c], David W. McLaughlin[d,e,f,g,h,1], Douglas Zhou[a,b,c,1], and Songting Li[a,b,c,1]

Affiliations are included on p. 10.

Contributed by David McLaughlin; received May 15, 2025; accepted August 29, 2025; reviewed by Stephen Coombes and Dario L. Ringach

Neurons process information by integrating thousands of synaptic inputs along their dendrites. Understanding the computational principles underlying neuronal information processing requires a reliable measure of synaptic conductance dynamics that accurately represents the input sources before signal integration and processing. Prevailing approaches to measuring synaptic conductances typically employ a voltage clamp at the soma of a neuron and assume the neuron as an isopotential point when processing electrical signals. However, owing to the presence of the well-known space clamp effect, the measurement of synaptic conductances through these methods often leads to significant errors, impeding the elucidation of dendritic signal features and subsequent signal integration processes. To address this issue, here we first develop a two-step clamp method at the soma that separately recovers the mean and time constant information of local synaptic conductance on the dendrite with high accuracy when a neuron receives a single synaptic input. Furthermore, under in vivo conditions of multiple synaptic inputs, we propose an intercept method to extract effective net excitatory and inhibitory synaptic conductances from measurements of synaptic currents at the soma. Both methods are grounded in mathematical perturbation analyses of a conductance-based passive cable model and are validated across multiple biologically detailed multicompartment neuron models with active channels, including Purkinje neuron, pyramidal neuron, and fast-spiking interneuron. Results demonstrate that our methods effectively circumvent the space clamp effect, offering reliable means to assess the role of measured conductances and synaptic activity in neuronal information processing.

conductance measurement | local synaptic conductance | effective conductance | space clamp effect

Significance

Neurons communicate by activating synapses along dendrites. To decipher the principles of neuronal coding, it is essential to recover input signals before they integrate at the soma. Traditional approaches, which often utilize a somatic voltage clamp, typically assume a neuron is electrotonically compact. However, the assumption is increasingly challenged by both theoretical and experimental studies due to the significant measurement error it introduces. Here, we develop methods of conductance measurement that, while still employing the somatic voltage clamp, effectively circumvent the space clamp effect. The methods enable accurate recovery of both local dendritic conductance and effective conductances at the soma, offering a reliable way to discern synaptic input information and assess its impact on neuronal information processing.

Neuronal networks operate via a complex interplay of excitatory (E) and inhibitory (I) inputs, often exhibiting a fluctuation-driven, balanced E–I dynamics. For each neuron within a network, disentangling its E from I inputs is crucial for elucidating the regulation of E-I balance and dendritic input integration. The commonly used experimental techniques for E and I input conductance measurements use current injections at the soma to clamp the somatic voltage at preselected values (1–11). Unfortunately, such clamping methods are notoriously unreliable, at times even producing estimates of negative conductances (12). The source of this unreliability is termed the "space clamp effect"—that while the voltage at the soma can be clamped to a prescribed value, the voltage cannot be clamped uniformly throughout the incoming dendritic arbor (13, 14). Since the clamping method is based on the false assumption that the soma and incoming dendritic arbor are isopotential, it is crucial to clarify and quantify the impact of this isopotential assumption on the measurement of E and I conductances in order to develop a more accurate measurement technique.

Here, we first develop a perturbation analysis framework and mathematically quantify the detailed mechanisms underlying the space clamp effect for an idealized ball-and-stick neuron model (the soma connects to an unbranched dendrite), and then use computational simulations to extend these theoretical results to several realistic neuron models with complex dendritic morphologies and a variety of ion channels. More specifically, our perturbation analysis enables the following: i) The proposal of a two-step clamp method to identify characteristics of local conductances (at locations along the dendritic arbor) based on somatic measurements. These characteristics include the temporal mean of the local conductances, as well as their rise and decay time constants. ii) The identification and quantification of those interactions between the clamp current and the synaptic currents that underlie the space clamp effect. iii) A precise definition of biologically relevant effective E and I somatic conductances (G_E^{eff}, G_I^{eff}) that intrinsically quantify the influence of synaptic inputs on somatic responses. iv) The proposal of a stable method,

Author contributions: Z.W., D.W.M., D.Z., and S.L. designed research; performed research; analyzed data; and wrote the paper.

Reviewers: S.C., University of Nottingham; and D.L.R., University of California, Los Angeles.

The authors declare no competing interest.

[1]To whom correspondence may be addressed. Email: david.mclaughlin@nyu.edu, zdz@sjtu.edu.cn, or songting@sjtu.edu.cn.

This article contains supporting information online at https://www.pnas.org/lookup/suppl/doi:10.1073/pnas.2512294122/-/DCSupplemental.

Published October 3, 2025.

termed the "intercept method," to determine G_E^{eff} and G_I^{eff} from clamping measurements at the soma—a method whose accuracy can be estimated with our perturbation analysis. Thus, this study proposes a reliable method to estimate local and effective somatic conductances with perturbative error estimates. Our methods could be implemented via the voltage clamp methods that are very similar to the traditional experimental clamping method. Notably, our methods could be further extended to the current clamp methods and provide a reliable approach to evaluate the contribution of measured conductances and synaptic activity to neuronal information processing.

Recovery of the Local Synaptic Conductance. First, we use a perturbation analysis to develop a two-step method based on a voltage clamp at the soma to effectively recover local synaptic dynamics, including conductances. The first step recovers the temporal mean value of the local conductance and the second step recovers its rise and decay time constants. Note that the input strength can be inferred from the temporal mean of the conductance once the time constants are estimated. Subsequently, the temporal profile of the local synaptic conductance dynamics can be estimated. We emphasize that, while the perturbation results are derived for an ideal neuron with an unbranched dendrite, we show through numerical simulations that the results are accurate for realistic neuron models with complex dendritic morphologies and various ionic dynamics.

Recovery of the mean of the local synaptic conductance. For the sake of illustration, we begin by studying an ideal neuron with an unbranched dendrite, receiving a single E synaptic input at the dendritic location $x = x_E$ at time $t = 0$. [The analysis can be straightforwardly extended to the case of inhibitory input and branched dendrites (15, 16).] In addition, a clamp current is injected into the soma of the neuron to maintain a fixed somatic voltage, initiated from $t = -\infty$. This preparatory step, starting the voltage clamp sufficiently early before the synaptic input, guarantees that the somatic membrane potential reaches the steady state of the clamping voltage before the synaptic input arrives. According to the cable neuron model (17), which treats neuronal dendrites as long, thin cylinders and thus represents the underlying three-dimensional dendritic structure in one dimension (18), the neural dynamics obey Eq. **1**,

$$c\frac{\partial v(x,t)}{\partial t} = -g_L v(x,t) + \frac{d}{4r}\frac{\partial^2 v(x,t)}{\partial x^2} - I^{\text{syn}} + I^{\text{cla}}, \quad [1]$$

where c and g_L denote the capacitance and the leak conductance per unit area of the membrane, respectively; r and d represent the axial resistivity and diameter of the dendrite, respectively. The synaptic current $I^{\text{syn}} = g_E(t)\delta(x - x_E)(v - \varepsilon_E)$ is given at location x_E with reversal potential ε_E, and the clamp current $I^{\text{cla}} = I^{\text{inj}}(t)\delta(x - x_S)$ is given at the soma. $\delta(x)$ denotes the Dirac Delta function. The local excitatory conductance $g_E(t) = f_E u_E(t)$, where f_E is the input strength, and u_E is the normalized E conductance modeled as in ref. 19 $u_E(t) = N_E(e^{-\frac{t}{\tau_{Ed}}} - e^{-\frac{t}{\tau_{Er}}})$, where τ_{Er} and τ_{Ed} are the rise and decay time constants. The peak value of u_E is normalized to unity by the normalization factor $N_E = [(\frac{\tau_{Er}}{\tau_{Ed}})^{\frac{\tau_{Er}}{\tau_{Ed}-\tau_{Er}}} - (\frac{\tau_{Er}}{\tau_{Ed}})^{\frac{\tau_{Ed}}{\tau_{Ed}-\tau_{Er}}}]^{-1}$. Boundary conditions are given by (20, 21)

$$c\frac{\partial v(0,t)}{\partial t} = -g_L v(0,t) + \frac{\pi d^2}{4Sr}\frac{\partial v}{\partial x}\Big|_{x=0}, \qquad \frac{\partial v}{\partial x}\Big|_{x=L} = 0, \quad [2]$$

where L is the length of dendrite, and S is the area of soma.

In general, an individual excitatory postsynaptic potential has a small amplitude (22, 23), indicating relatively small input strength f_E. Therefore, we expand both the somatic response and clamp current in terms of the small parameter f_E, i.e.,

$$I^{\text{inj}}(t) = \sum_{m=0}^{\infty} f_E^m I_m^{\text{inj}}(t), \quad v(x,t) = \sum_{m=0}^{\infty} f_E^m v_m(x,t). \quad [3]$$

By substituting Eq. **3** into Eq. **1**, and arranging the equations by their respective orders, we can obtain an ordered hierarchy of equations. Focusing on the zeroth order, we have

$$c\frac{\partial v_0}{\partial t} = -g_L v_0 + \frac{d}{4r}\frac{\partial v_0^2}{\partial x^2} + I_0^{\text{inj}}\delta(x - x_S). \quad [4]$$

Note that the Green's function $\Gamma(x, y, t)$ is defined as the solution of Eq. **1**, with the clamp and synaptic currents replaced by pulse input $\delta(x - y)\delta(t)$, that satisfies the boundary conditions Eq. **2**; and it can be found analytically (20, 21). With Green's function, the analytic solution to Eq. **4** can be expressed as

$$v_0(x,t) = \Big(\int_0^{\infty} \Gamma(x, x_S, \eta)\, d\eta\Big) I_0^{\text{inj}}. \quad [5]$$

The zeroth-order solution $v_0(x, t)$ is time-independent, highlighting the somatic voltage clamp's efficacy in maintaining the somatic membrane potential at a fixed level through the injection of current I_0^{inj}. Given its time-invariant property, $v_0(x, t)$ is subsequently denoted as $v_0(x)$.

Notably, the integral enclosed in the parenthesis in Eq. **5** can be viewed as the Laplace transform of $\Gamma(x, x_S, t)$ at frequency $s = 0$, denoted as $\mathcal{L}\{\Gamma\}(x, x_S, 0)$. This interpretation allows us to delineate the membrane potential at the dendritic location $x = x_E$ as

$$v_0(x_E) = K_E v_0(x_S), \quad [6]$$

where the factor $K_E = \mathcal{L}\{\Gamma\}(x_E, x_S, 0)[\mathcal{L}\{\Gamma\}(x_S, x_S, 0)]^{-1}$. The factor denotes the deviation of membrane potential at the synaptic location from somatic voltage and is just the ratio of the response kernel at the synaptic location to that at the soma. Note that the factor K_E can be quite small and is independent of the magnitude of the clamped current. Such findings cast doubt upon a traditional assumption that treats the neuron as isopotential. Further simulations of a neocortical layer 5 pyramidal neuron validate a substantial discrepancy between dendritic and somatic voltages. As depicted in Fig. 1*A*, the discrepancy can reach up to 20 mV, highlighting the spatial heterogeneity of neuronal signaling.

At first-order $\mathcal{O}(f_E)$, Eq. **1** becomes

$$c\frac{\partial v_1}{\partial t} = -g_L v_1 + \frac{d}{4r}\frac{\partial^2 v_1}{\partial x^2} - I_1^{\text{syn}}\delta(x - x_E) + I_1^{\text{inj}}\delta(x - x_S), \quad [7]$$

where $I_1^{\text{syn}} = u_E(t)(v_0(x) - \varepsilon_E)$. Note that, in the voltage clamp mode, the somatic membrane potential remains clamped at the predetermined level $v_0(x_S)$. Consequently, Eq. **7** is constrained by the condition $v_1(x_S, t) = 0$. Thus, representing the solution of Eq. **7** with the Green's function $\Gamma(x, y, t)$ yields:

$$\Gamma(x_S, x_S, t) * I_1^{\text{inj}}(t) = \Gamma(x_S, x_E, t) * I_1^{\text{syn}}(x_E, t), \quad [8]$$

where $*$ denotes temporal convolution. Note that, under the voltage clamp mode, we can estimate the synaptic current arriving

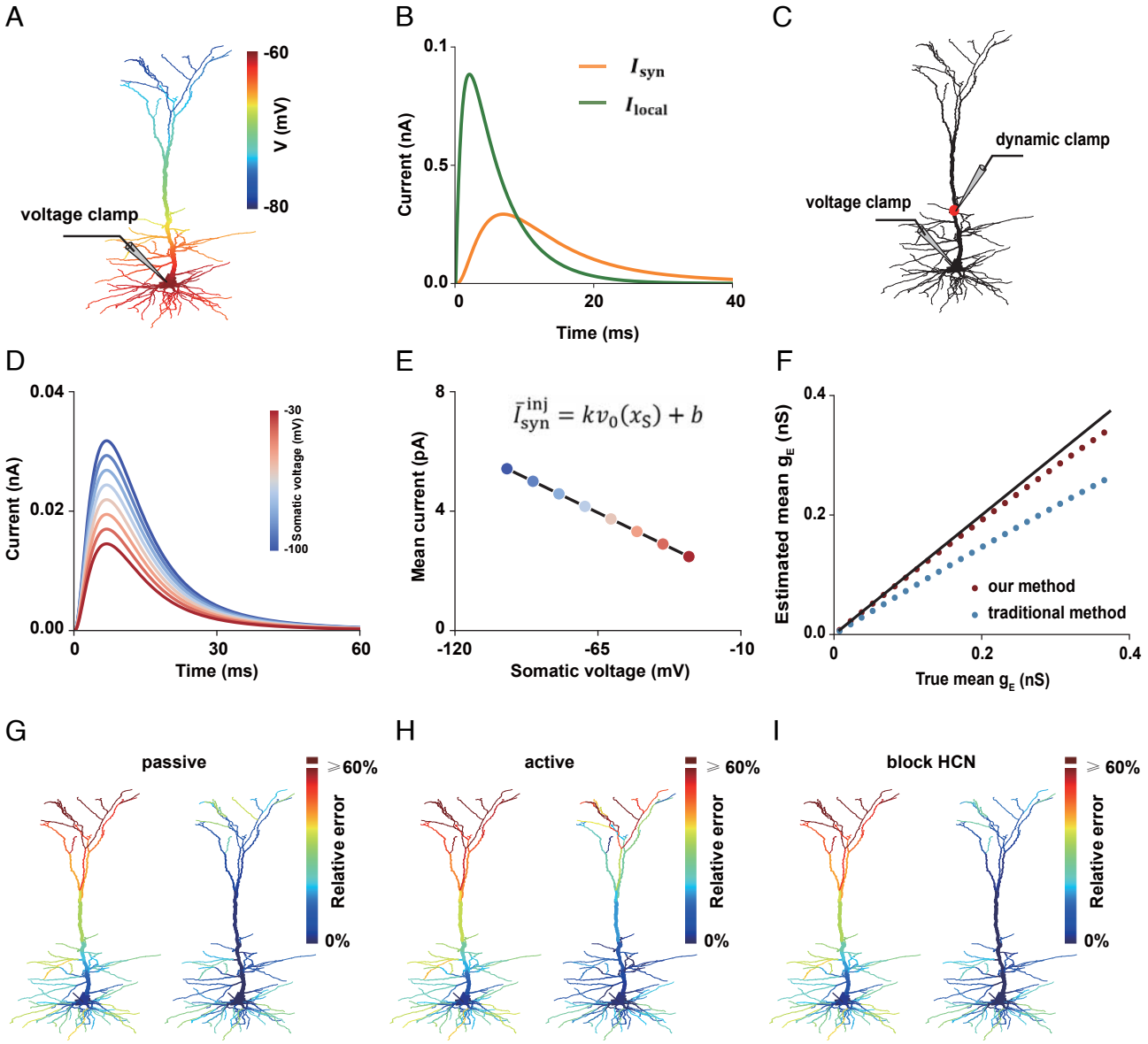

Fig. 1. Recovery of mean local synaptic conductance in a realistic neocortical layer 5 pyramidal neuron model. (*A*) Voltage distribution in the pyramidal neuron model under a somatic voltage clamp set at −60 mV. (*B*) The notable discrepancy between the local synaptic current and the synaptic current measured at the soma when the input is given at 300 μm from the soma. (*C–E*) Illustrate the recovery process using our method. (*C*) Depicts the simulation setup, wherein a dynamic clamp is applied at the dendrite to mimic synaptic input, alongside a somatic voltage clamp. (*D*) Shows the synaptic current at the soma, measured under distinct clamped somatic voltages. (*E*) The mean synaptic current measured at the soma exhibits a linear relationship with the somatic voltage, enabling recovery of mean local synaptic conductance based on the slope and intercept. (*F*) Comparison of mean local synaptic conductance recovery by our method and the traditional method against the true mean local synaptic conductance. The EPSP amplitude induced at 300 μm from the soma ranges from about 0.1 to 3.5 mV. (*G*) Spatial dependence of the relative error for mean local synaptic conductance measurement by the traditional method (*Left*) versus our method (*Right*) in the passive pyramidal neuron model, with *E* input strength fixed at each location. (*H*) Similar to (*G*), but with active ion channels included. (*I*), Similar to (*H*) but with the HCN channel blocked.

at the soma, denoted as I_{syn}^{inj}, from the change of the clamp current, i.e., $I_{syn}^{inj} = -f_E I_1^{inj} + \mathcal{O}(f_E^2)$. Consequently, by multiplying f_E to both sides of Eq. **8**, applying the Laplace transform to Eq. **8** and setting $s = 0$ yields a linear relationship between measured synaptic current at the soma and the clamping voltage as

$$\bar{I}_{syn}^{inj} = -K_E^2 \cdot \bar{g}_E \cdot v_0(x_S) + K_E \cdot \bar{g}_E \cdot \varepsilon_E + \mathcal{O}(f_E^2), \quad [9]$$

where we define $\bar{h} = \int_0^\infty h(\tau)d\tau$ for any integrable function $h(t)$, in particular $\bar{I}_{syn}^{inj} = \int_0^\infty I_{syn}^{inj}(\tau)d\tau$ and $\bar{g}_E = \int_0^\infty g_E(\tau)\,d\tau$ represent the total synaptic charge and the aggregate conductance, respectively. Note that Eq. **9** can be reformulated as

$$\bar{I}_{syn}^{inj} = K_E \bar{g}_E(\varepsilon_E - v_0(x_E)), \quad [10]$$

which shows that, as the local synaptic current diffuses across the dendrites, the local synaptic current undergoes attenuation owing to factors like resistive flow and leakage, as depicted in Fig. 1*B*. This attenuation leads to a discrepancy between the actual synaptic current measured at the soma and the actual local current at the location of the synapse $\bar{g}_E(\varepsilon_E - v_0(x_E))$. This discrepancy arises from the space clamp effect and is captured here by the fact that $K_E < 1$, with the $1 - K_E$ an estimate of the size of the space clamp effect.

Notably, using Eq. **9**, despite the space clamp effect (i.e., $K_E <$ 1), it is possible to estimate accurately the aggregate synaptic

conductance $\bar{g}_E$. To be specific, one can clamp the somatic voltage at multiple levels, and fit the linear relationship between the holding potential $v_0(x_S)$ and the corresponding total synaptic charge $\bar{I}_{\text{syn}}^{\text{inj}}$ to obtain $\bar{I}_{\text{syn}}^{\text{inj}} = kv_0(x_S) + b$, where the slope k and the intercept b (obtained by linear regression) produce

$$k = -K_E^2 \cdot \bar{g}_E, \quad [11]$$

$$b = K_E \cdot \bar{g}_E \cdot \varepsilon_E. \quad [12]$$

Utilizing the Eqs. **11** and **12**, one can recover the aggregate synaptic conductance as

$$\bar{g}_E = -\frac{b^2}{k} \cdot \frac{1}{\varepsilon_E^2}. \quad [13]$$

In general, the conductance change lasts for a finite duration, typically, in tens of milliseconds. This characteristic permits estimation of mean local synaptic conductance by dividing $\bar{g}_E$ by the duration time T. Considering that EPSPs usually last for 47.6 ± 18.2 ms (24), we set $T = 100$ ms in our subsequent simulations.

Our approach for determining accurately the mean local synaptic conductance is showcased in Fig. 1 using simulations of a neocortical layer 5 pyramidal neuron with both passive and active dendrites cases (31). We first consider the scenario of passive dendrites, where cable theory is an exact description of its dynamics. Specifically, we analyze an E synaptic input located 300 μm away from the soma on the dendritic trunk, as shown in Fig. 1*C*. By applying a voltage clamp at the soma, we can adjust the magnitude of the holding somatic voltage while repeating the local synaptic input to measure the synaptic current under varying holding potentials, as illustrated in Fig. 1 *C* and *D*. Consistent with the prediction of Eq. **9**, the mean synaptic current shows a linear relation with the holding potential, as shown in Fig. 1*E*. Our method effectively recovers the mean local synaptic conductance by exploiting the linear relationship given by Eq. **13**. In addition, as depicted in Fig. 1*F* for an E input and *SI Appendix*, Fig. S1*A* for an I input, our method is robustly applicable across a wide range of synaptic input strengths. Our approach consistently outperforms the traditional method based on the point neuron assumption (i.e., $K_E = 1$), which estimates the local synaptic conductance by $g_E = I_{\text{syn}}^{\text{inj}}[\varepsilon_E - v_0(x_S)]^{-1}$. The average relative error (relative error $= \frac{|\hat{g}-g^*|}{g^*}$, where $\hat{g}$ is an estimation of g^*) of our method is 10% for an E synaptic input across all dendrites. In contrast, the traditional method can incur an average relative error of up to 26% across all dendrites. Additionally, when an E synaptic input is located far away from the soma, the estimation error of the traditional method can exceed 60%, whereas our method continues to exhibit small relative error, as depicted in Fig. 1*G*. For the case of an I synaptic input, the traditional method performs even poorer with an average relative error of 32%. In comparison, our method maintains an average relative error of 10% across all dendrites, as illustrated in *SI Appendix*, Fig. S1*B*. However, we note that at certain dendritic tips, the relative error of our method increases slightly due to dendritic escape effects (see *SI Appendix* for detailed error analysis).

Next, we assess the impact of active conductances on our method by simulations with a variety of voltage-gated conductances. Incorporation of the active conductances results in a slight decline in precision (average relative error of our method: 14% for an E input and 10% for an I input), as shown in Fig. 1*H* and *SI Appendix*, Fig. S1*C*. This decrease in accuracy is primarily attributed to the distortion of synaptic current by active conductances. Despite this, it is noteworthy that our method consistently outperforms the traditional approach, as illustrated in Fig. 1*H* and *SI Appendix*, Fig. S1*C*.

To improve the accuracy of our method in the presence of active channels, we investigate the influence of each channel on the method's precision. This investigation reveals that most active conductances exhibit minimal influence on our estimation of mean local synaptic conductance. The exception is the HCN current, a type of cation ion current that significantly diminishes the accuracy of our estimation. However, blocking HCN channels restores the high accuracy of our estimation (average relative error of our method: 9% for an E input, 10% for an I input), while the performance of the traditional method barely improves (average relative error of the traditional method: 26% for an E input, 32% for an I input), as illustrated in Fig. 1*I* for the case of an E input and *SI Appendix*, Fig. S1*D* for that of an I input. In physiological experiments, specific compounds can indeed be used to selectively block HCN channels, as demonstrated by Balducci et al. (25).

Recovery of the time constants of the local synaptic conductance. The second step of our method is accomplished by changing the onset time of the somatic voltage clamp to recover local synaptic time constants—an approach motivated by the "voltage jump method" previously developed (26). We first describe the method analytically for a single input (E or I) on an idealized dendrite and then show the method's generality through numerical simulations.

In a manner akin to recovering the mean local synaptic conductance, we consider the scenario where an E synaptic input is delivered to a dendritic location $x = x_E$ at time $t = 0$. In addition, rather than starting from $t = -\infty$, the clamp current is now initiated at $t = \xi > 0$ after the arrival of the synaptic input. Consequently, this adjustment changes the solution of Eq. **7**, as the term $v_0(x)$ in I_1^{syn} becomes time-dependent. This time dependence arises from the delay in clamp current initiation, resulting in $I_1^{\text{syn}} = u_E(t)(v_0(x,t) - \varepsilon_E)$. In addition, the clamp current starts to counteract the synaptic current only after $t = \xi$. Hence, the membrane potential at the soma, $v_1(x_S, t)$, is nonzero until $t = \xi$, allowing the EPSP at the soma to be measured before the clamp's influence takes effect. With the Green's function, we obtain:

$$v_1(x_S, t) = \Gamma(x_S, x, t) \star [-I_1^{\text{syn}}\delta(x - x_E) + I_1^{\text{inj}}\delta(x - x_S)], \quad [14]$$

where $\star$ denotes spatiotemporal convolution. Multiplying f_E to both sides of Eq. **14** and using the first-order approximation of the synaptic current at the soma $I_{\text{syn}}^{\text{inj}} = -f_E I_1^{\text{inj}} + \mathcal{O}(f_E^2)$ and the somatic EPSP $V_E(t) = f_E v_1(x_S, t) + \mathcal{O}(f_E^2)$, we obtain:

$$\Gamma(x_S, x_S, t) * I_{\text{syn}}^{\text{inj}}(t) + V_E(t) = -\Gamma(x_S, x_E, t) * [f_E I_1^{\text{syn}}(t)].$$

By performing the Laplace transform on both sides of the above equation and setting $s = 0$, we obtain

$$\bar{I}_{\text{syn}}^{\text{inj}} + F(V_E) = -K_E \overline{\bar{g}_E v_0}(x_E) + R, \quad [15]$$

where $F(V_E) = \bar{V}_E[\bar{\Gamma}(x_S, x_S)]^{-1}$ and the reminder term $R = K_E \bar{g}_E \varepsilon_E + \mathcal{O}(f_E^2)$. Again, here we define $\bar{h} = \int_0^\infty h(\tau)d\tau$ for any integrable function $h(t)$. It is important to point out that $v_0(x_E, t) = 0$ when $t < \xi$ because $v_0(x_E, t)$ is induced by the clamp current I_0^{inj}, which starts at $t = \xi$ in our

settings. Consequently, the following equality holds, $v_0(x_E, t) = v_0(x_E)\Theta(t-\xi)$, where $\Theta(t)$ is the Heaviside function. Therefore, the term on the right-hand side of Eq. **15** manifests as a double exponential function $H(\xi) = w_1 e^{-\frac{\xi}{\tau_{Ed}}} + w_2 e^{-\frac{\xi}{\tau_{Er}}}$ with parameters of the synaptic time constants τ_{Er} and τ_{Ed} (see details in *SI Appendix*), and Eq. **15** reduces to

$$\bar{I}_{\text{syn}}^{\text{inj}} + F(V_E) = H(\xi; \tau_{Er}, \tau_{Ed}) + R. \qquad \textbf{[16]}$$

Eq. **16** suggests a method to recover the time constants of local synaptic conductance. By varying the starting time of the voltage clamp $t = \xi$ in different trials, τ_{Er} and τ_{Ed} can be estimated by fitting the quantity on the left-hand side of Eq. **16** using the format of $H(\xi; \tau_{Er}, \tau_{Ed}) + const$. Note that all components on the left-hand side of Eq. **16** are experimentally measurable. For example, the synaptic current $I_{\text{syn}}^{\text{inj}}$ is equal to the difference between the total clamp current I^{inj} and the baseline current I_0^{inj}, where the baseline current I_0^{inj} can be measured by initiating the voltage clamp at $t = \xi$ in the absence of the synaptic input. In addition, the EPSP response at the soma V_E can be recorded prior to the onset of the voltage clamp. The term $\bar{\Gamma}(x_S, x_S)$ in the expression of $F(V_E)$ represents the input resistance at the soma, which can be calculated by the ratio of the magnitude of clamped membrane potential to the injected current in the absence of any synaptic input.

Fig. 2 provides a numerical validation of the recovery method of the local synaptic time constants, employing the neocortical layer 5 pyramidal neuron model with passive and active dendrites (31). We first consider the scenario of passive dendrites. We note that, if the membrane potential is initially clamped at its resting state at $t = -\infty$ and subsequently switched to a different level at $t = \xi$, as illustrated in Fig. 2*A*, then the term V_E in Eq. **16** will vanish. In this special scenario, our method is simplified to the voltage jump method previously developed (26). Accordingly, for convenience, we use this method in our simulations. As predicted by Eq. **16**, the measured synaptic charge is well described by a double exponential function of ξ, exhibiting time constants nearly identical to those of local synaptic conductance. This is demonstrated in Fig. 2*B*, where the estimated rise time constant is 1.08 ms (compared to the ground truth of 1 ms), and the estimated decay time constant is 5.01 ms (with a ground truth of 5 ms). In addition, the method accurately extracts the rise and decay time constants of local synaptic conductance across a diverse range of input strengths, as shown in Fig. 2*C* for an *E* input and *SI Appendix*, Fig. S2*A* for an *I* input (estimated rise time constants: 1.0 to 1.2 ms for an *E* input case, 1.0 to 1.8 ms for an *I* input case; Estimated decay time constants: 5.0 to 5.2 ms for an *E* input case, 5.0 to 5.5 ms for an *I* input case). The input, positioned on the dendritic trunk 300 μm away from the soma, spans the amplitude of EPSPs ranging from about 0.1 to 3.5 mV. Moreover, our method can accurately estimate the synaptic time constants even when synaptic input is positioned far away from the soma, as depicted in Fig. 2*D* for an *E* input and *SI Appendix*, Fig. S2*B* for an *I* input.

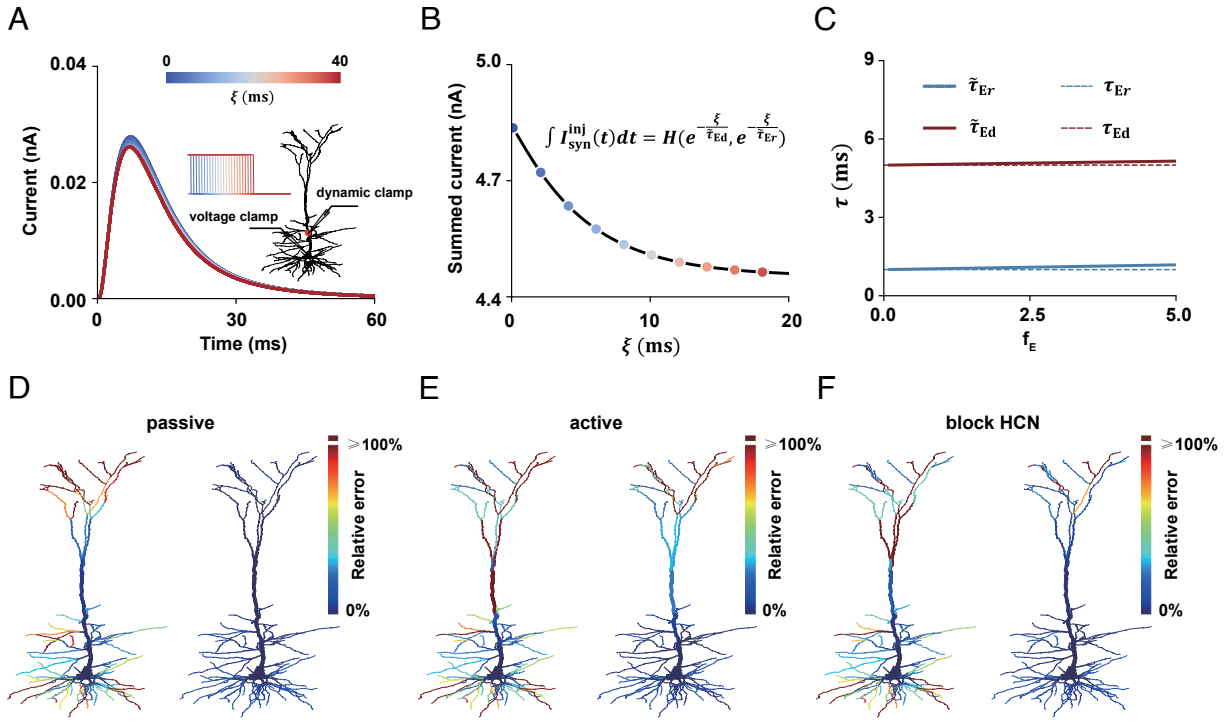

Fig. 2. Recovery of local synaptic time constants in the realistic neocortical layer 5 pyramidal neuron model. (*A* and *B*), illustrate the recovery process using our method. (*A*) Depicts the simulation setup, a dynamic clamp is applied at the dendrite to mimic synaptic input, alongside a somatic voltage clamp. The resulting synaptic current is estimated and recorded as the somatic voltage clamp amplitude changes at $t = \xi$, with different colors representing distinct values of ξ. The *Inset* curve shows the corresponding somatic voltage. (*B*) Demonstrates that the synaptic charge exhibits a double exponential function concerning the change time ξ. The black curve is derived from fitting using exponential functions, i.e., $H(\xi) = w_1 e^{-\frac{\xi}{\tilde{\tau}_{Ed}}} + w_2 e^{-\frac{\xi}{\tilde{\tau}_{Er}}} + w_3$, following the algorithm in ref. 27. $\tilde{\tau}_{Ed}$ and $\tilde{\tau}_{Er}$ are the estimation of synaptic time constants. (*C*) Comparison of the estimated and true synaptic time constants for the *E* input, spanning EPSP amplitudes from about 0.1 to 3.5 mV. (*D*) The spatial dependence of the relative error in synaptic time constants measurement for the *E* input in the passive pyramidal neuron, with input strength fixed at each location. The *Left* panel shows the relative error in synaptic rise time constant estimation, and the *Right* panel exhibits the relative error in synaptic decay time constant estimation. (*E*) Is similar to (*D*) but includes active ion channels. (*F*) Similar to (*E*) but with the HCN channel blocked.

Furthermore, in the presence of diverse active conductances, our method remains highly effective for synapses located near the basal dendrites. However, its accuracy declines significantly for synapses positioned on distal apical dendrites, as illustrated in Fig. 2*E* for an *E* input and *SI Appendix*, Fig. S2*C* for an *I* input. This decline is primarily attributed to the small diameter of the distal apical dendrites, which results in increased dendritic escape and, consequently, greater truncation errors. For further details, see the error analysis in *SI Appendix*. Notably, selectively blocking *only* the HCN channel type substantially improves our estimates for both *E* and *I* inputs, as demonstrated in Fig. 2*F* for an *E* input and *SI Appendix*, Fig. S2*D* for an *I* input. In contrast, blocking other ion channels has minimal impact on our estimates.

Recovery of the Effective Conductance at the Soma. Under in vivo conditions, a neuron receives many synaptic inputs that are widely distributed over its dendritic arbors. In such a case, it is unrealistic to attempt to isolate and recover the local synaptic conductance of each synapse. Nonetheless, it remains possible to quantitatively measure the total effective *E* and *I* conductances at the soma. These effective conductances are biologically meaningful and important as they directly determine the generation of action potentials. Previous works (1–11) assumed that the effective *E* and *I* conductances can be straightforwardly separated from the total synaptic current using the traditional voltage clamp method—under an assumption that the synaptic current measured under the voltage clamp mode accurately captures the synaptic input signals, independent of the clamping voltage. However, as we next show, asymptotic analysis of the cable neuron model establishes a significant interaction between the clamp current and the synaptic current. This interaction arises from the space clamp effect and leads to significant discrepancies between the conductances measured by the traditional voltage clamp method and the actual effective conductances at the soma. Based on our analysis and simulations, we further propose an alternative strategy for analyzing clamp data, which is able to accurately separate and recover the effective *E* and *I* conductances. With numerical simulations for a wide range of realistic neuron models characterized by complex dendritic morphologies and diverse ionic dynamics, we demonstrate the method's accurate capturing of effective synaptic conductances—with much more accuracy than the traditional method.

Interaction between clamp current and synaptic current. In the framework of the point-neuron model, it is conventionally assumed that all synaptic currents, along with the injected current, are linearly summed at the soma. However, this summation is oversimplified as the injected current at the soma can alter the dendritic membrane potential, leading to a nonlinear interaction between the injected current and the synaptic current. As a result, these currents can not be simply summed linearly at the soma and conductance measured by the traditional method depends on the clamped somatic voltage, as we will now demonstrate analytically with the cable model.

To leading order in f_E, Eq. **8** can be rewritten, using the expressions for the injected current at the soma $I_{\rm syn}^{\rm inj} = -f_E I_1^{\rm inj} + \mathcal{O}(f_E^2)$, for the synaptic current at the dendrite $I_1^{\rm syn} = u_E(t)(v_0(x_E) - \varepsilon_E)$ and for $v_0(x_E) = K_E v_0(x_S)$ (from Eq. **6**), as

$$I_{\rm syn}^{\rm inj}(t) = \mathcal{L}^{-1}\{k_E(s)\cdot\mathcal{L}\{g_E\}(s)\}(\varepsilon_E - K_E v_0(x_S)) + \mathcal{O}(f_E^2), \quad [17]$$

where $k_E(s) = \mathcal{L}\{\Gamma\}(x_S, x_E, s)[\mathcal{L}\{\Gamma\}(x_S, x_S, s)]^{-1}$.

In the absence of clamp current, the total current arriving at the soma, denoted by $I_{\rm total}(t)$, is defined as the effective synaptic current $I_{\rm syn}^{\rm eff}$. Furthermore, according to Eq. **5**, the zeroth order of somatic voltage is zero, i.e., $v_0(x_S) = 0$. Substituting this condition into Eq. **17** yields

$$I_{\rm total}(t) = I_{\rm syn}^{\rm eff}(t) = \mathcal{L}^{-1}\{k_E(s)\cdot\mathcal{L}\{g_E\}(s)\}\,\varepsilon_E + \mathcal{O}(f_E^2). \quad [18]$$

When an injected current is concurrently applied at the soma, the voltage on the whole dendrite is altered. In this case, the space clamp effect (characterized by $K_E < 1$) introduces an additional interaction current $I_{\rm syn}^{\rm int}$. Therefore, the total current arriving at the soma comprises the injected current, the effective synaptic current, and the interaction current:

$$\begin{aligned} I_{\rm total}(t) &= I_0^{\rm inj} + I_{\rm syn}^{\rm eff} + I_{\rm syn}^{\rm int} + \mathcal{O}(f_E^2),\\ I_{\rm syn}^{\rm eff}(t) &= \mathcal{L}^{-1}\{k_E(s)\cdot\mathcal{L}\{g_E\}(s)\}(\varepsilon_E - v_0(x_S)),\\ I_{\rm syn}^{\rm int}(t) &= \mathcal{L}^{-1}\{k_E(s)\cdot\mathcal{L}\{g_E\}(s)\}(1-K_E)v_0(x_S). \end{aligned} \quad [19]$$

Therefore, the presence of the space clamp effect, indicated by $K_E < 1$, introduces an interaction term such that the total current arriving at the soma cannot be described as merely the linear sum of the effective synaptic current and the injected current, as shown in Fig. 3*A*.

In the traditional approach, the injected current is assumed to induce only a change in the membrane potential at the synapse, which does not affect the conductance measurement. Therefore, the excitatory conductance can be measured as

$$G_E^{\rm inj} = \frac{I_{\rm total} - I_0^{\rm inj}}{\varepsilon_E - v(x_S)}, \quad [20]$$

where $I_{\rm total}(t)$ and $I_0^{\rm inj}$ can be measured via voltage clamp, and $v(x_S)$ is the holding somatic voltage. However, by Eq. **19**, we have

$$G_E^{\rm inj} = \frac{I_{\rm syn}^{\rm eff} + I_{\rm syn}^{\rm int}}{\varepsilon_E - v_0(x_S)} + \mathcal{O}(f_E^2), \quad [21]$$

which depends on the clamped somatic voltage $v_0(x_S)$ due to the interaction, contradicting the traditional assumption. The superscript in $G_E^{\rm inj}$ underscores the *E* conductance measured in the presence of an injected current. Similar results hold for the *I* synaptic input case.

Next, we validate the existence of the interaction between the clamp current and the synaptic current via the simulation of the realistic layer 5 pyramidal neuron model (31). These numerical results confirm the significance of the interaction of the two currents on the determination of the conductance $G_E^{\rm inj}$. For instance, with an individual *E* synaptic input located at a dendritic site distant from the soma, together with a voltage clamp at the soma, we can numerically obtain the synaptic current $I_{\rm syn}^{\rm inj}$. By adjusting the magnitude of the holding somatic voltage while maintaining the strength of the local synaptic input, one can obtain the corresponding synaptic current $I_{\rm syn}^{\rm inj}$ with different amplitudes, as shown in Fig. 3*B*. As predicted by our theoretical analysis in Eq. **17**, a linear dependence of the measured peak amplitude of the synaptic current $I_{\rm syn}^{\rm inj}$ on the holding somatic voltage $v_0(x_S)$ is shown in Fig. 3*C*.

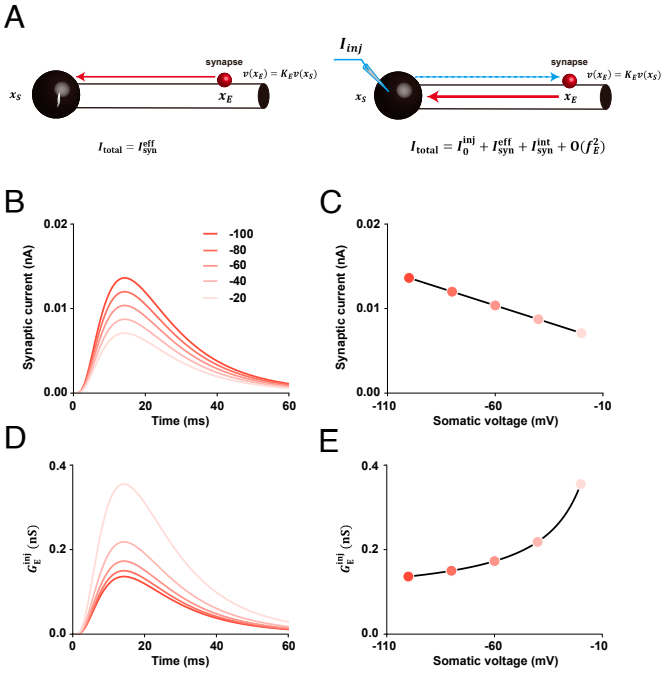

Fig. 3. Interaction between the injected current and the excitatory synaptic current in the passive pyramidal neuron model. (*A*) Schematic of interaction. *Left* panel: an *E* input is applied at $x = x_E$. The local synaptic current propagates through the dendrite and reaches the soma. The total current arriving at the soma is the effective synaptic current, as given by Eq. **18**. *Right* panel: an injected current is applied at the soma together with a synaptic current applied at x_E, altering the dendritic voltage. The space clamp effect $K_E < 1$ results in an interaction current, as shown in Eq. **19**. Consequently, the total current at the soma is not the linear sum of the effective synaptic current and the clamp current. (*B*) Measured effective *E* synaptic current in the neuron model with a somatic voltage clamp. The color indicates the holding somatic voltage. (*C*) Linear dependence of the peak amplitude of the *E* synaptic current on the somatic voltage. (*D*) The temporal profile of G_E^{inj} numerically measured under the same situation in (*B*). (*E*) Nonlinear dependence of the peak amplitude of G_E^{inj} on the somatic voltage. For (*B*–*E*), an individual *E* pulse input is given at the location on the dendrite 300 μm away from the soma. (*B*–*E*) Share the same color-coded legend. In (*C*) and (*E*), dots are values obtained from numerical simulation, and solid curves are the predictions from the first-order perturbation analysis of the cable neuron by Eqs. **17** and **21**.

The *E* conductance G_E^{inj} under somatic voltage clamp can then calculated using Eq. **21**. Contrary to the common belief that the synaptic conductance measured at the soma is approximately independent of the holding potential by the voltage clamp, the simulation result shows a significant dependency of the *E* conductance on the clamped somatic voltage, as depicted in Fig. 3 *D* and *E*. The discrepancy between the peak *E* conductance G_E^{inj} measured in the presence of the injected current and the *E* conductance defined in the absence of injected current ranges from about 4% to a substantial level of 150%. In fact, the difference can be arbitrarily large as the magnitude of the injected current further increases. Similarly, as shown in *SI Appendix*, Fig. S3, the disparity between the peak *I* conductance G_I^{inj} measured by the traditional voltage clamp method and the *I* conductance measured in the absence of injected current can also be quite pronounced. Notably, as depicted in *SI Appendix*, Fig. S3*D*, the traditional method can estimate a negative value of the *I* conductance under certain magnitudes of the injected current.

Owing to the nonlinear relationship between G_E^{inj}, G_I^{inj} and the injected clamp current, the assumption of the linear summation of the synaptic currents arriving at the soma and the clamp current at the soma is not valid. As a consequence, a reformulation of the point-neuron model at the soma is required to account for the interactions, since the conductances G_E^{inj} and G_I^{inj} are dependent on I^{inj}. This underscores that, even in the presence of only one type (either *E* or *I*) of synaptic input, the conventional estimate of conductance is questionable and requires a new approach to recover the true conductances.

Effective conductance measurement under the voltage clamp. In this section, we introduce a method to accurately estimate effective conductances (both excitatory and inhibitory) from voltage clamp data. We first illustrate the method for an excitatory *E* (or inhibitory *I*) input. Subsequently, we generalize this approach to scenarios involving multiple synaptic inputs.

First, we make an explicit definition of the effective conductance G_E^{eff}, and then use a perturbation analysis to give a method of estimating the effective conductance from measurements at the soma. When the neuron receives an excitatory input on the dendrite, the effective conductance $G_E^{\text{eff}}(t)$ is defined as a conductance at the soma that produces the same somatic response:

$$\begin{aligned} v(x_S, t) &= \Gamma(x_S, x_E, t) * [g_E(t)(\varepsilon_E - v(x_E, t))] \\ &= \Gamma(x_S, x_S, t) * [G_E^{\text{eff}}(t)(\varepsilon_E - v(x_S, t))]. \end{aligned} \quad [22]$$

To analyze Eq. **22**, we expand $v(x, t)$ and $G_E^{\text{eff}}(t)$ as series with respect to the input strength f_E, i.e.,

$$v(x, t) = \sum_{m=1}^{\infty} f_E^m v_m(x, t), \quad G_E^{\text{eff}}(t) = \sum_{m=1}^{\infty} f_E^m h_m^{\text{eff}}(t).$$

Substituting the above series into Eq. **22** yields the first-order expression

$$\Gamma(x_S, x_E, t) * u_E(t) = \Gamma(x_S, x_S, t) * h_1^{\text{eff}}(t). \quad [23]$$

Multiply both sides of Eq. **23** by f_E and perform the Laplace transform. Subsequently, using the first-order approximation of the effective conductance $G_E^{\text{eff}}(t) = f_E h_1^{\text{eff}}(t) + \mathcal{O}(f_E^2)$, one obtains:

$$\mathcal{L}\{G_E^{\text{eff}}\}(s) = \frac{\mathcal{L}\{\Gamma\}(x_S, x_E, s)}{\mathcal{L}\{\Gamma\}(x_S, x_S, s)} \mathcal{L}\{g_E\}(s) + \mathcal{O}(f_E^2). \quad [24]$$

Eq. **24** establishes the relationship between the local synaptic conductance g_E and the effective conductance G_E^{eff} in the Laplace domain. Similarly, we can obtain the effective *I* conductance when a neuron receives an *I* input,

$$\mathcal{L}\{G_I^{\text{eff}}\}(s) = \frac{\mathcal{L}\{\Gamma\}(x_S, x_I, s)}{\mathcal{L}\{\Gamma\}(x_S, x_S, s)} \mathcal{L}\{g_I\}(s) + \mathcal{O}(f_I^2). \quad [25]$$

Furthermore, when a neuron receives multiple *E* or *I* inputs, to the leading order, the concept of the total effective conductance can be generalized as a linear summation of the individual *E* or *I* inputs.

Next, we develop a method to recover the effective conductances G_E^{eff} and G_I^{eff} when both *E* and *I* inputs are presented. In the cable model of Eq. **1**, a clamp current is injected into the soma starting from $t = -\infty$ described by $I^{\text{cla}} = I^{\text{inj}}(t)\delta(x - x_S)$. Subsequently, a pair of *E* and *I* synaptic inputs are delivered to the neuron at time $t = 0$ at the synaptic locations $x = x_E$ and $x = x_I$, respectively with $I^{\text{syn}} = \sum_{q=E,I} f_q u_q(t)\delta(x - x_q)(v - \varepsilon_q)$.

The clamp current and membrane potential can be asymptotically expanded in terms of f_E and f_I,

$$I^{\text{inj}}(t) = \sum_{k=0}^{\infty} \sum_{m+n=k}^{\infty} f_E^m f_I^n I_{mn}(t),$$
$$v(x,t) = \sum_{k=0}^{\infty} \sum_{m+n=k}^{\infty} f_E^m f_I^n v_{mn}(x,t). \quad [26]$$

Under the voltage clamp mode, the synaptic current reaching the soma is estimated from changes in the clamp current. Specifically, the relationship is given by

$$I_{\text{syn}}^{\text{inj}} = -(I^{\text{inj}}(t) - I_{00}) = -\sum_{k=1}^{\infty} \sum_{m+n=k}^{\infty} f_E^m f_I^n I_{mn}(t).$$

Therefore, by representing $I_{\text{syn}}^{\text{inj}}$ as $-f_E I_{10} - f_I I_{01} + \mathcal{O}(f^2)$, and incorporating Eqs. **24** and **25**, we obtain

$$\mathcal{L}\{I_{\text{syn}}^{\text{inj}}\}(s) = \mathcal{L}\{G_E^{\text{eff}}\}(s)\hat{V}_E + \mathcal{L}\{G_I^{\text{eff}}\}(s)\hat{V}_I + \mathcal{O}(f^2), \quad [27]$$

where $\hat{V}_q = \varepsilon_q - K_q v_{00}(x_S)$ denotes the driving force of q-type synapse, and $K_q = \mathcal{L}\{\Gamma\}(x_q, x_S, 0)[\mathcal{L}\{\Gamma\}(x_S, x_S, 0)]^{-1}$, with $q = E, I$. By applying the inverse Laplace transform to Eq. **27**, a linear I–V relationship is deduced at each time point, i.e.,

$$I_{\text{syn}}^{\text{inj}}(t) = k(t)V^{\text{cla}} + b(t) + \mathcal{O}(f^2),$$

where $V^{\text{cla}} = v_{00}(x_S)$ denotes the clamped somatic voltage. Accordingly, the slope is

$$k = -K_E G_E^{\text{eff}} - K_I G_I^{\text{eff}}, \quad [28]$$

and the intercept is

$$b = G_E^{\text{eff}}\varepsilon_E + G_I^{\text{eff}}\varepsilon_I. \quad [29]$$

The traditional voltage clamp method attempts to measure G_E^{eff} and G_I^{eff}, under the assumption that the clamped voltage is uniformly distributed from soma to dendrite, and produces formulas for the current at the soma that are similar to Eqs. **28** and **29**, except with K_E= 1 and K_I = 1. Since K_E and K_I are not equal to 1 (and often can be less than 1), the traditional method gives inaccurate estimates of the effective conductances at the soma. Moreover, the effective conductances as estimated by the traditional method lack a clear biological meaning; hence, errors in measuring effective conductances in the traditional method cannot be eliminated, even with minimal clamp current. This limitation will be further demonstrated by the forthcoming simulation results below.

Because the prefactors K_E and K_I depend on the locations of synaptic inputs, they cannot be determined without knowledge of the synaptic locations—a situation that becomes increasingly complex when a neuron receives numerous inputs across its dendritic tree. However, the relationship between the intercept and effective conductances provides a stable foundation for measuring the effective E and I conductances, that does not depend explicitly upon K_E and K_I. Given that there are two unknowns G_E^{eff} and G_I^{eff}, it is required to obtain at least one additional intercept equation. This can be achieved by blocking either the E or I synaptic inputs (28). For example, if the I inputs are blocked, a second intercept equation can be obtained

$$b' = G_E^{\text{eff}}\varepsilon_E.$$

Consequently, by utilizing the two intercept equations, the effective E and I conductances can be determined. We term this procedure the intercept method.

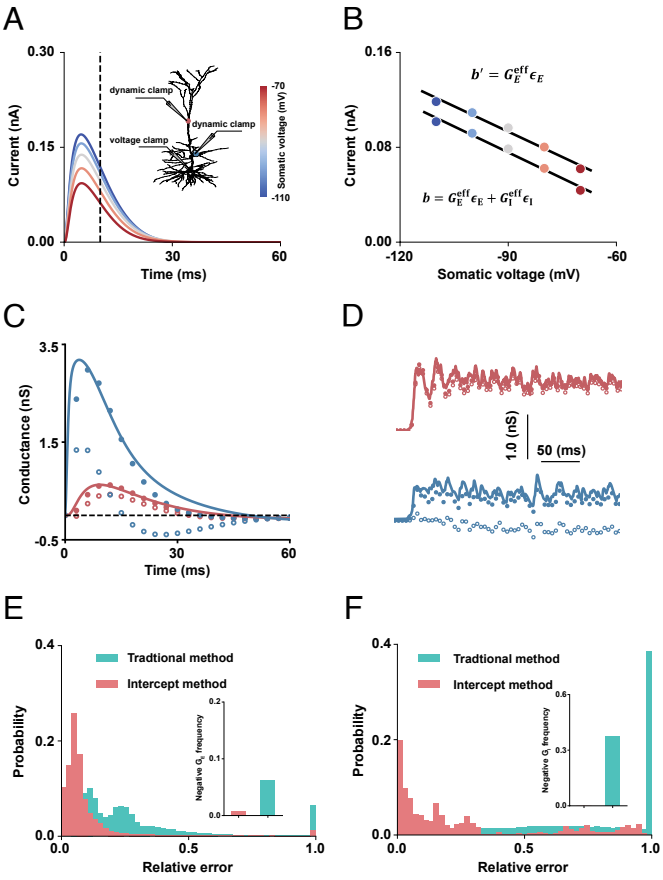

Fig. 4. Determination of effective conductance in the realistic active pyramidal neuron model with somatic voltage clamp. (*A*) The estimation process of our method. Two dynamic clamps are applied at the dendrites to mimic a pair of synaptic inputs, red for an *E* input and blue for an *I* input, alongside a somatic voltage clamp. The estimated synaptic current varies with the somatic voltage; the corresponding somatic voltage is indicated by color. For the sake of illustration, we select $t = 10$ ms (vertical dashed line) to extract the synaptic current at that time point. In (*B*), the extracted synaptic current is plotted against the somatic voltage, with the black curve resulting from a linear fit. This allows for the accurate estimation of the effective *E* and *I* conductances based on the intercept. (*C* and *D*) The effective *E* conductance (solid red dots) and *I* conductance (solid blue dots) determined by the intercept method are relatively close to the true values of the effective *E* (red line) and *I* (blue line) conductances, whereas the *E* conductance (open red circle) and the *I* conductance (open blue circle) measured by the traditional method deviate greatly from the true values. The deviation is particularly significant for the *I* case. (*C*) is for the case of a pair of *E* and *I* transient inputs located on the dendrites 580 μm and 200 μm away from the soma, respectively. *Inset* in *C* is the schematic diagram of the recording configuration. The dashed parallel line indicates the zero-conductance baseline. (*D*) Is for the case of multiple inputs of 80 *E* and 20 *I* locations distributed across the entire dendritic tree with the rate of 40 Hz at each synaptic input site. (*E* and *F*), the distribution of relative errors in conductance measurements. For these measurements, the locations for a pair of *E* and *I* synaptic inputs are scanned across the entire dendritic tree. The *Insets* illustrate the frequency of occurrences where the measured mean conductance is negative. (*E*) Represents the results for *E* conductance. While (*F*) shows the results for *I* conductance. For ease of presentation, when plotting histograms, any error values exceeding 1 are capped at 1 in the statistical representation. The *E* and *I* reversal potentials are $\varepsilon_E = 90$. mV, $\varepsilon_I = -10$. mV relative to the resting potential, respectively.

It is straightforward to extend these results to scenarios where a neuron receives multiple E and I synaptic inputs. Under a first-order approximation, the total effective E and I conductance can be considered as the linear summation of the conductances from individual E and I inputs. Based on the linear superposition principle, the effective conductance in such a case can be recovered from two intercept equations given by

$$b = G^{\text{eff}}_{\text{total }E}\epsilon_E + G^{\text{eff}}_{\text{total }I}\epsilon_I,$$

$$b' = G^{\text{eff}}_{\text{total }E}\epsilon_E,$$

where $G^{\text{eff}}_{\text{total }E}$ and $G^{\text{eff}}_{\text{total }I}$ represent the effective conductances for total E and I inputs, respectively.

The effectiveness of the intercept method under the voltage clamp mode has been numerically validated and illustrated in Fig. 4. When a pair of E and I synaptic inputs are simultaneously received by the pyramidal neuron model with active ionic channels, we measure the resultant synaptic current $I^{\text{inj}}_{\text{syn}}$ by varying the somatic potential via voltage clamp, as depicted in Fig. 4*A*. (31) The synaptic current at each time point indeed shows a linear relation with the somatic voltage, as indicated in Fig. 4*B*, allowing us to obtain the corresponding intercept through linear fitting. Moreover, by blocking the I synaptic input, an additional intercept is obtained. Combining these two intercept equations enables us to estimate the effective E and I conductances, as illustrated in Fig. 4*B*. In addition, in Fig. 4*C*, the conductances measured using the intercept method exhibit small relative errors of 20% for E conductance and 24% for I conductance, while the errors made by the traditional method based on both slope and intercept information can reach up to 45% for E conductance and 77% for I conductance. The result demonstrates the effectiveness of the intercept method over the traditional method. Notably, at certain time points, the conductances estimated by the traditional method even yield negative values, as shown in Fig. 4*C*, reminiscent of the traditional data analysis of some early experiments (29) (For a detailed discussion on the underlying reasons for these negative conductance measurements, please refer to *SI Appendix*).

To simulate in vivo conditions, we set 80 E inputs and 20 I inputs broadly distributed across the entire dendritic tree of the neuron model. The arrival time of each synaptic input is randomly assigned between 0 and 1,000 ms with an input rate of 40 Hz. In these simulations, the intercept method well approximates the true effective conductances with small relative errors of 8% for E conductance and 13% for I conductance. In contrast, the conductances estimated by the traditional method greatly deviate from the true values, particularly for inhibitory inputs. The relative error for the traditional method reaches 32% for E conductance and 128% for I conductance.

We further explore how the accuracy of the two methods is influenced by the location of synaptic inputs. We systematically vary the positions of synaptic inputs across all possible dendritic sites. Our simulations indicate that, for a pair of E and I inputs, the intercept method maintains an average relative error of around 12% for E conductance and 25% for I conductance. In contrast, the error associated with the traditional method is quite large, reaching 39% for E conductance and 132% for I conductance, as depicted in Fig. 4 *E* and *F* (Note that, in Fig. 4*F*, error values greater than 1 are capped at 1 for visual clarity in the statistical representation. However, the true error values are used to compute the average relative error). Additionally, the traditional method often results in negative mean conductance values, further highlighting its limitations.

Discussion

In previous studies, the estimation of E and I conductances and currents was based on the traditional method using a voltage clamp. The method infers conductances from a linear I–V relationship, where the slope represents the negative of the total conductance and the intercept denotes the reversal current (1–11). However, due to the space clamp effect, conductances determined by the traditional method inevitably deviate from their true value and lack biological interpretation. In this work, we have proposed methods to recover synaptic input features via theoretical analysis of an idealized cable model, extended to realistic pyramidal neurons by numerical simulations. When a neuron receives a single synaptic input, our two-step clamp method enables the accurate extraction of the mean local synaptic conductance as well as their rise and decay time constants. We also explicitly define effective excitatory and inhibitory somatic conductances that are biologically meaningful, and from the definition, calculate the effective conductances perturbatively. Realizing these perturbation calculations under voltage clamp leads to the introduction of an intercept method to estimate excitatory and inhibitory effective somatic conductances from somatic voltage clamping measurements. Moreover, this intercept method is shown by numerical simulations to accurately recover the effective excitatory and inhibitory conductances when a neuron receives multiple synaptic inputs distributed across its dendritic arbors. These approaches effectively circumvent the significant distortions in the kinetics of synaptic currents caused by the space clamp effect. In addition, our methods employ the voltage clamp to recover synaptic conductances, thus avoiding somatic spike and subsequent contamination of synaptic conductance estimates by intrinsic currents (30).

It is important to stress that we have shown, through simulations involving a realistic neuron model, that our method consistently achieves high accuracy in estimating local synaptic conductance and effective conductances. Accuracy holds true over a broad range of synaptic input strengths, synaptic input locations, ionic channels, and receptors. However, two factors can significantly degrade the accuracy of our estimations: i) large EPSPs and ii) active channels of HCN type. First, if the EPSP is too large, it invalidates the accuracy of first-order perturbation theory and necessitates higher-order corrections. Typically, EPSPs are weak; however, synaptic inputs located at dendritic tips elicit larger EPSPs, as do synapses located on thin dendrites. In these situations, first-order methods are not sufficient for accuracy (more details in *SI Appendix*). Second, one channel type (HCNs) significantly degrades the method. However, blocking HCN channels, as demonstrated in ref. 25, restores the high accuracy of the method.

By leveraging asymptotic analysis, our framework transforms the nonlinear cable equation into an ordered hierarchy of linear equations. This linearization enables the use of Green's function to establish an accurate relationship between somatic current and synaptic conductance. Notably, our analytical framework is independent of specific neuronal morphology. Therefore, for neurons with arbitrary and complex dendritic architectures, the Green's function can be derived using the established sum-over-trips formalism (15, 16). Taken together, these features allow for the extension of our method to neurons with complex, branched dendritic trees. Alternatively, we extend our methods by using numerical simulations of the neocortical layer 5 pyramidal neuron with branched dendrites, as shown in Figs. 1–4 in the main text. In addition, we also perform numerical simulations of the medial prefrontal cortex fast-spiking neurons (32), cerebellar Purkinje neurons (33), and hippocampal pyramidal neurons (34). In each

case, our methods recover local synaptic conductance dynamics and effective conductances with high accuracy, as shown in *SI Appendix*, Figs. S4–S10.

Our numerical simulations confirm that the proposed methods provide accurate estimates of both local and effective synaptic conductances across a variety of neuronal morphologies and dynamics. However, implementing these approaches in practical experimental settings requires several conditions. Specifically: i) Achieving the two-step clamp and intercept methods requires precise control of both the timing and location of synaptic inputs in repeated trials, and it requires multiple somatic voltage clamp recordings at distinct holding potentials, demanding stable patch-clamp access across successive trials; ii) The intercept method depends on selective pharmacological isolation of E or I inputs; iii) Some endogenous active dendritic conductances (e.g., HCN channels) may induce strong nonlinear interactions that can compromise conductance recovery unless these currents are blocked. In light of current electrophysiological and pharmacological methodologies, our method is most reliably applied in in vitro preparations-such as acute brain slices or dissociated neuron cultures-where precise voltage control, input manipulation, and modulation of dendritic channel activity are routinely attainable. Nevertheless, we believe that our approaches hold future potential for in vivo applications, such as studying E–I interactions driven by external sensory inputs, provided the experimental techniques meet these required conditions under in vivo settings.

Data, Materials, and Software Availability. All data in this study were generated from numerical simulations. The simulation codes used to produce the results have been deposited in GitHub and are publicly available at https://github.com/Vivian-wang-maker/conductance-measurement/tree/main (35). The models implemented in this study include neocortical layer 5 pyramidal (31), the medial prefrontal cortex fast-spiking neurons (32), cerebellar Purkinje neurons (33), and hippocampal pyramidal neurons (34). All other data are included in the article and/or *SI Appendix*.

ACKNOWLEDGMENTS. This work was supported by National Key R&D Program of China 2023YFF1204200, Science and Technology Commission of Shanghai Municipality with Grant No. 24JS2810400 (Z.W., D.Z., and S.L.); National Natural Science Foundation of China with Grant Nos. 12225109 and 12071287 (D.Z.); National Natural Science Foundation of China Grants 12271361 and 12250710674 (S.L.), and the Student Innovation Center at Shanghai Jiao Tong University (Z.W., D.Z., and S.L.).

Author affiliations: [a]School of Mathematical Sciences, Shanghai Jiao Tong University, Shanghai 200240, China; [b]Institute of Natural Sciences, Shanghai Jiao Tong University, Shanghai 200240, China; [c]Ministry of Education Key Laboratory of Scientific and Engineering Computing, Shanghai Jiao Tong University, Shanghai 200240, China; [d]Courant Institute of Mathematical Sciences, New York University, New York, NY 10012; [e]Center for Neural Science, New York University, New York, NY 10012; [f]Institute of Mathematical Sciences, New York University Shanghai, Shanghai 200122, China; [g]New York University Tandon School of Engineering, New York University, Brooklyn, NY 11201; and [h]Neuroscience Institute of New York University Langone Health, New York University, New York, NY 10016

1. L. Borg-Graham, C. Monier, Y. Fregnac, Voltage-clamp measurement of visually-evoked conductances with whole-cell patch recordings in primary visual cortex. *J. Physiol.* **90**, 185–188 (1996).
2. L. J. Borg-Graham, C. Monier, Y. Fregnac, Visual input evokes transient and strong shunting inhibition in visual cortical neurons. *Nature* **393**, 369–373 (1998).
3. N. Le Roux, M. Amar, G. Baux, P. Fossier, Homeostatic control of the excitation-inhibition balance in cortical layer 5 pyramidal neurons. *Eur. J. Neurosci.* **24**, 3507–3518 (2006).
4. B. V. Atallah, W. Bruns, M. Carandini, M. Scanziani, Parvalbumin-expressing interneurons linearly transform cortical responses to visual stimuli. *Neuron* **73**, 159–170 (2012).
5. L. I. Zhang, A. Y. Tan, C. E. Schreiner, M. M. Merzenich, Topography and synaptic shaping of direction selectivity in primary auditory cortex. *Nature* **424**, 201–205 (2003).
6. M. Wehr, A. M. Zador, Balanced inhibition underlies tuning and sharpens spike timing in auditory cortex. *Nature* **426**, 442–446 (2003).
7. M. Wehr, A. M. Zador, Synaptic mechanisms of forward suppression in rat auditory cortex. *Neuron* **47**, 437–445 (2005).
8. Cq. Ye, Mm. Poo, Y. Dan, Xh. Zhang, Synaptic mechanisms of direction selectivity in primary auditory cortex. *J. Neurosci.* **30**, 1861–1868 (2010).
9. Y. Shu, A. Hasenstaub, D. A. McCormick, Turning on and off recurrent balanced cortical activity. *Nature* **423**, 288–293 (2003).
10. B. Haider, A. Duque, A. R. Hasenstaub, D. A. McCormick, Neocortical network activity in vivo is generated through a dynamic balance of excitation and inhibition. *J. Neurosci.* **26**, 4535–4545 (2006).
11. S. J. Cruikshank, T. J. Lewis, B. W. Connors, Synaptic basis for intense thalamocortical activation of feedforward inhibitory cells in neocortex. *Nat. Neurosci.* **10**, 462–468 (2007).
12. C. Monier, J. Fournier, Y. Frégnac, In vitro and in vivo measures of evoked excitatory and inhibitory conductance dynamics in sensory cortices. *J. Neurosci. Methods* **169**, 323–365 (2008).
13. J. C. Magee, Dendritic integration of excitatory synaptic input. *Nat. Rev. Neurosci.* **1**, 181–190 (2000).
14. N. Spruston, Pyramidal neurons: Dendritic structure and synaptic integration. *Nat. Rev. Neurosci.* **9**, 206–221 (2008).
15. B. J. Cao, L. F. Abbott, A new computational method for cable theory problems. *Biophys. J.* **64**, 303–313 (1993).
16. L. F. Abbott, Simple diagrammatic rules for solving dendritic cable problems. *Physica A* **185**, 343–356 (1992).
17. W. Rall, Theory of physiological properties of dendrites. *Ann. N. Y. Acad. Sci.* **96**, 1071–1092 (1962).
18. K. A. Lindsay, J. R. Rosenberg, G. Tucker, From Maxwell's equations to the cable equation and beyond. *Prog. Biophys. Mol. Biol.* **85**, 71–116 (2004).
19. C. Koch, *Biophysics of Computation: Information Processing in Single Neurons* (Oxford University Press, 2004).
20. S. Li, D. Zhou, D. Cai, Analysis of the dendritic integration of excitatory and inhibitory inputs using cable models. *Commun. Math. Sci.* **13**, 565–575 (2015).
21. S. Li, D. W. McLaughlin, D. Zhou, Mathematical modeling and analysis of spatial neuron dynamics: Dendritic integration and beyond. *Commun. Pure Appl. Math.* **76**, 114–162 (2023).
22. J. C. Magee, E. P. Cook, Somatic EPSP amplitude is independent of synapse location in hippocampal pyramidal neurons. *Nat. Neurosci.* **3**, 895–903 (2000).
23. S. R. Williams, G. J. Stuart, Dependence of EPSP efficacy on synapse location in neocortical pyramidal neurons. *Science* **295**, 1907–1910 (2002).
24. B. Sutor, J. J. Hablitz, EPSPs in rat neocortical neurons in vitro. I. Electrophysiological evidence for two distinct EPSPs. *J. Neurophysiol.* **61**, 607–620 (1989).
25. V. Balducci *et al*., The HCN channel as a pharmacological target: Why, where, and how to block it. *Prog. Biophys. Mol. Biol.* **166**, 173–181 (2021).
26. M. Häusser, A. Roth, Estimating the time course of the excitatory synaptic conductance in neocortical pyramidal cells using a novel voltage jump method. *J. Neurosci.* **17**, 7606–7625 (1997).
27. JGB, Fit sum of exponentials (Mathematics Stack Exchange) (version: 2020-08-31). https://math.stackexchange.com/q/3808325/; https://math.stackexchange.com/users/605948/juan-gonzalezburgos. Accessed 13 September 2025.
28. L. A. Atherton, E. S. Burnell, J. R. Mellor, Assessment of methods for the intracellular blockade of gabaa receptors. *PLoS ONE* **11**, e0160900 (2016).
29. S. R. Williams, S. J. Mitchell, Direct measurement of somatic voltage clamp errors in central neurons. *Nat. Neurosci.* **11**, 790–798 (2008).
30. A. Guillamon, D. W. McLaughlin, J. Rinzel, Estimation of synaptic conductances. *J. Physiol.* **100**, 31–42 (2006).
31. E. Hay, S. Hill, F. Schümann, H. Markram, I. Segev, Models of neocortical layer 5b pyramidal cells capturing a wide range of dendritic and perisomatic active properties. *PLOS Comput. Biol.* **7**, e1002107 (2011).
32. A. Tzilivaki, G. Kastellakis, P. Poirazi, Challenging the point neuron dogma: FS basket cells as 2-stage nonlinear integrators. *Nat. Commun.* **10**, 3664 (2019).
33. S. Masoli, S. Solinas, E. D'Angelo, Action potential processing in a detailed Purkinje cell model reveals a critical role for axonal compartmentalization. *Front. Cell. Neurosci.* **9**, 47 (2015).
34. S. Li, N. Liu, X.-H. Zhang, D. Zhou, D. Cai, Bilinearity in spatiotemporal integration of synaptic inputs. PLOS *Comput. Biol.* **10**, e1004014 (2014).
35. Z. Wang, Conductance measurement. GitHub. https://github.com/Vivian-wang-maker/conductance-measurement/tree/main. Accessed 16 September 2025.